Available online at www.sciencedirect.com

ScienceDirect

Ceramics International 40 (2014) 1635–1639

CERAMICS INTERNATIONAL

www.elsevier.com/locate/ceramint

Er doped ZnO nanoplates: Synthesis, optical and dielectric properties

Reza Zamiri*, Ajay Kaushal, Avito Rebelo, J.M.F. Ferreira

Department of Materials and Ceramic Engineering, CICECO, University of Aveiro, 3810-193 Aveiro, Portugal

Received 3 June 2013; received in revised form 9 July 2013; accepted 10 July 2013
Available online 18 July 2013

Abstract

We report on synthesis of rare earth Er doped ZnO nanoplates via low cost wet precipitation method. The effect of varying Er doping concentration in the range from 3, 5 to 7 wt% on structural, optical and electrical properties of ZnO nanoplates has been successfully investigated. X-ray diffraction (XRD) studies show hexagonal wurtzite phase structure of prepared Er doped ZnO nanoplates. Scanning electron microscopy (SEM) reveals the growth of nanoplates like structures of the prepared samples. Further, the presence of Er ions doping in ZnO matrix has been confirmed by EDS measurement. A sharp and strong peak at around 435 cm^{-1} was observed in Raman spectra of nanoplates which correspond to the high frequency branch of the E2 mode of ZnO. The frequency dependence of dielectric constant (ε_r), dielectric loss (tan δ) and AC conductivity of ZnO nanoplates of different Er doping concentration were measured. The dielectric properties of pure and Er doped ZnO nanoplates follow a behavior based on Maxwell–Weigner model. The AC conductivity was found to decrease with Er doping.

Keywords: C. Dielectric properties; Raman spectroscopy; ZnO nanoplates

1. Introduction

ZnO as an *n*-type semiconductor material has many applications such as gas sensors, varistors, piezoelectrics and as electrodes for solar cells [1–9]. On the other hand, it is well known that material properties change when transfers from bulk to nanostructures form leading to recent advances in ZnO nanostructures fabrications [10–13]. Dielectric constant and loss tangent are the most important properties of a material. The materials with high dielectric constant find numerous applications in microelectronics. AC measurements are important means for studying the dynamic properties, like conductance, capacitance, dielectric constant and dielectric loss tangent, of the semiconducting and dielectric materials. They provide information about interior of a material in the region of relatively low conductivity. ZnO is one of the potential candidates in the field of optoelectronics due to its high excitonic binding energy (60 meV), which depends on the dielectric constant of the materials. It is well known that the various properties of semiconductor material can be enhanced and/or modified on doping with proper ions in host lattice. Dielectric properties of ZnO have also been investigated earlier as per reports in literature [14]. Recently, improvement in dielectric behavior of ZnO has been reported on Co doping [15]. Aim of the present study is (i) to synthesize Er doped ZnO nanoplates via low cost wet precipitation method and (ii) to investigate the effect of varying Er doping concentration on various properties of ZnO nanoplates. The present investigations reveal that doping of rare earth Er in ZnO nanostructures is effective to change various structural, optical and electrical properties of ZnO.

2. Experiment

Er doped ZnO nanoplates with different Er doping concentrations of 3, 5 and 7 wt% were prepared by wet chemical precipitation method. $ZnCl_2$ (Sigma-Aldrich, Steinheim, Germany) and $Er(NO_3)_3 \cdot 6H_2O$ were used as Zn and Er precursors, respectively. Separate aqueous Zn and Er precursor

*Corresponding author. Tel.: +351 91 6759671.
E-mail addresses: rezaz@ua.pt, zamiri.r@gmail.com (R. Zamiri).

0272-8842/$ - see front matter © 2013 Elsevier Ltd and Techna Group S.r.l. All rights reserved.
http://dx.doi.org/10.1016/j.ceramint.2013.07.054

solutions of stoichiometric concentrations were prepared by dissolving in distilled water. Each of the as-obtained solutions were then dropped into 100 mL of 0.1 M NaOH (MERK) solution. The pH value of all the samples was kept constant to ~13 during the synthesis, leading to formation of precipitates. Further, the precipitates were washed several times with distilled water up to getting a Na^+ concentration below 0.66 ppm measured by atomic absorption spectroscopy. The as-obtained washed precipitates were then kept in oven for 24 h at temperature of 80 °C for drying. Finally, the dried powders were heat treated at temperature of 275 °C for 2 h.

The structural and surface morphology of the samples were studied by X-ray diffractometry (Shimadzu XRD-6000, Tokyo, Japan) and scanning electron microscopy (SEM). The optical properties of the samples were carried out by Raman spectrometry. For the measurement of electrical properties, the obtained powder was pressed to cylindrical shape disc of 10 mm diameter with thickness of ~2 mm and top conductive electrodes were deposited on both sides using silver paste. Dielectric constant and loss were measured at room temperature in wide frequency range from 100 Hz to 1 MHz, using an impedance analyzer (4294A, Agilent, USA).

3. Result and discussion

Fig. 1 shows the XRD patterns of pure and Er doped ZnO nanostructures with different Er doping concentrations of 3, 5 and 7 wt%. All the diffraction peaks correspond to hexagonal wurtzite phase in agreement with the respective Joint Committee on Powder Diffraction Standards (JCPDS) card no. 36-1451. It is worth noting that no additional peaks due to other oxide phases are present for all the prepared samples in the XRD pattern, indicating the phase purity of ZnO nanostructures. The absence of impurity peaks and the close matching with the hexagonal phase structure of as synthesized powder also suggests that the prepared samples are highly crystalline and the most of Er^{+3} ions incorporated into ZnO lattice through completely substituting instead of Zn^{2+} ions.

Fig. 2(a–d) shows the SEM images of prepared pure and Er doped ZnO nanostructures. SEM images reveal growth of

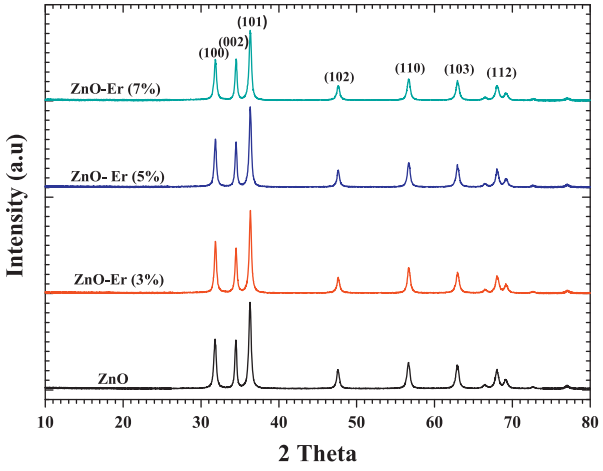

Fig. 1. The XRD patterns of pure and doped samples.

rod-like structures for pure ZnO (Fig. 2a), while the rod-like structures start getting emerged when doped with 3 wt% of Er in ZnO (Fig. 2b). Further increase of Er doping concentration to 5 and 7 wt% results in plate-like structural morphology (Fig. 2(c and d)). This systematic change of morphology from rod-like structures as observed in case of pure ZnO to plate-like structures indicates the effect of Er substitution in ZnO lattice. The results show the successful synthesis of plate-like structures of ZnO on Er doping. In ZnO, the high surface energy of the polar (0001) plane leads to faster crystal growth in *c*-axis direction of ZnO nanostructure favoring the formation of nano-rod shape structure along that direction. On the other hand, with incorporation of Er^{+3} in ZnO crystal lattice, the adsorption of hydroxide anion increased on the polar plane (0001) due to higher $q/r=3/0.89$ of Er^{+3} relative to $q/r=2/0.74$ of Zn^{+2}, which leads to partial reduction of crystal growth in *c*-axis. However, they can still grow sideways along $(2\overline{1}\overline{1}0)$ directions [16–18] as observed in case of 5 and 7 wt% Er doped samples (Fig. 2(c and d)). The presence of Er doping in ZnO was further confirmed by taking EDS spectra of the prepared samples. Fig. 3 shows the EDS spectra of pure and Er doped nanostructures shown in the corresponding SEM images (Fig. 2). The EDS spectra reveal the presence of O, Er, and Zn for doped samples. The presence of Cu signal observed is originated from TEM copper grid substrate used for EDS analysis with no other impurity signals has been detected in EDS spectra.

Raman spectroscopy was studied to see the effect of Er doping on vibrational properties of ZnO nanostructure. Fig. 4 shows the Raman spectra of pure and Er-doped ZnO nanostructures. The ZnO nanostructure with wurtzite hexagonal shape belongs to the P63mc symmetry group. Based on group theory it has eight sets of optical phonon modes at Γ point of the Brillouin zone, classified as 2B1 modes (Raman silent), A1 +E1 modes (infrared active) and A1+E1+2E2 modes (Raman active). Furthermore, the A1+E1modes are polar and split into the longitudinal optical [LO] and transverse optical phonons. The B1 modes are silent while E2 modes with two modes of low and high frequencies are Raman active. The sharp and strong peak at around 435 cm^{-1} has been observed in Raman spectra (Fig. 4), which could be attributed to the high frequency branch of the E2 mode of ZnO, and is a main Raman mode in the ZnO wurtzite crystal structure. It is related to the motion of oxygen atoms and sensitive to internal stress [19,20]. While the peak at about 576 cm^{-1} can be assigned to A1(LO) mode which is sensitive to changes in the free carrier concentrations [21] and might be caused due to Zn interstitials. The peak observed at 331 cm^{-1} frequency was assigned to second order vibration mode arising from the E2 (high)–E2 (low) multiple scattering process. The peaks at 375 and 100 cm^{-1} correspond to A1(TO) and E2L fundamental phonon modes of hexagonal ZnO, respectively. The peak at 204 cm^{-1} could be attributed to the 2E2L second-order phonon mode. Two additional phonon modes at 160 and 620 cm^{-1} have been observed in case of Er doped ZnO samples when compared to spectra of pure ZnO sample. According to the previous reports these two peaks might be

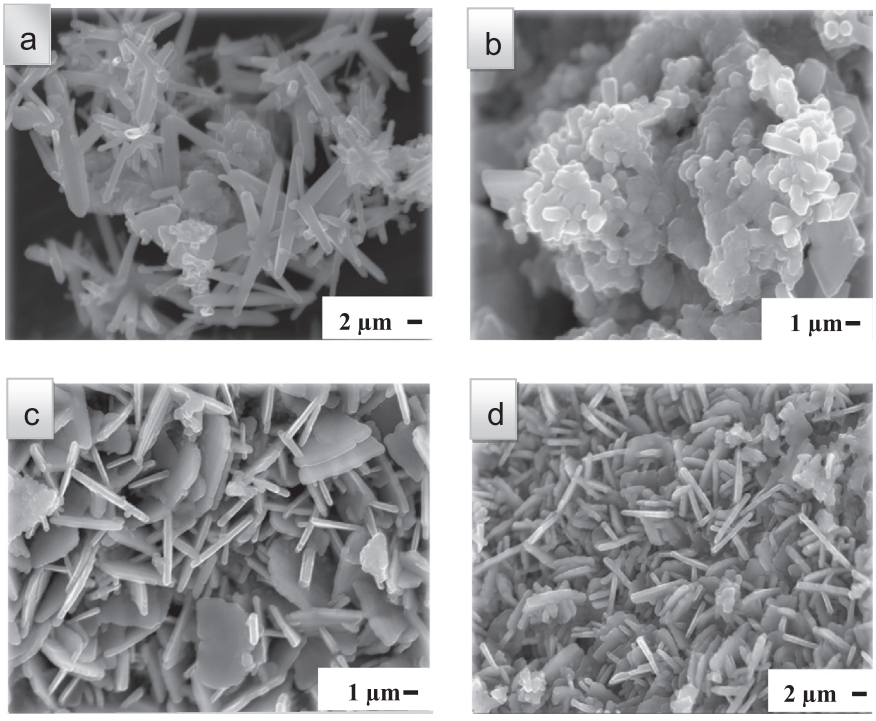

Fig. 2. SEM images of (a) pure and (b) (3 wt%), (c) (5 wt%) and (d) (7 wt%) Er doped ZnO samples.

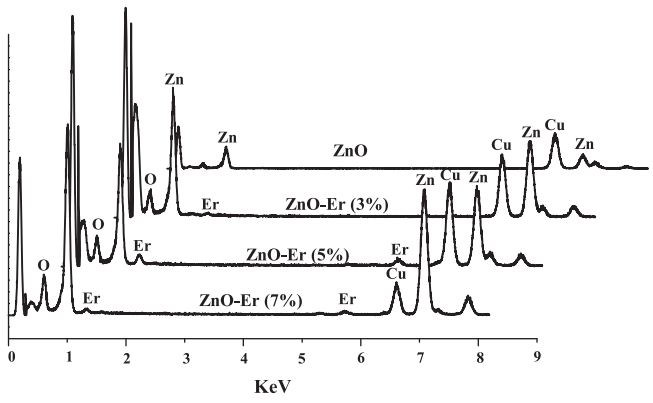

Fig. 3. EDS analysis of pure and Er-doped ZnO nanostructures.

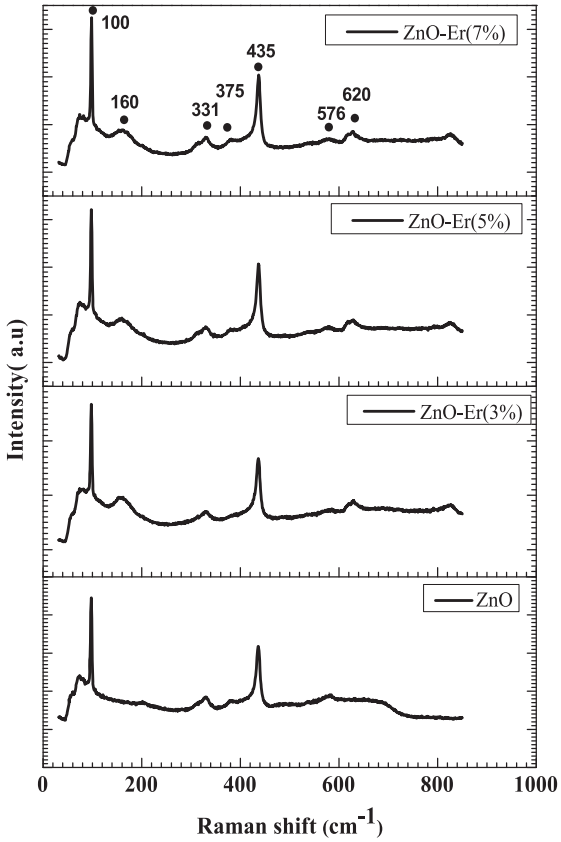

Fig. 4. Raman spectra of pure and Er-doped ZnO nanostructures.

related to the local vibration modes due to Er substitution in the ZnO host [22–24].

Fig. 5 shows the frequency dispersion of the dielectric constant (ε_r) values of pure and Er doped ZnO nanostructure, in the range from 1 kHz to 1 MHz measured at room temperature. Nanostructural powders were consolidated to disc shape for the electrical measurements without any further sintering of the compacts. All the samples exhibited minimal dispersion of ε_r as a function of the frequency. The value of ε_r decreased with increase in frequency. The trend of this decrement is rapid at low frequency and becomes slow at higher frequencies, approaching to frequency independent behavior. The dielectric dispersion behavior of the homogeneous double structure systems can be explained by Maxwell–Weigner model [25]. In this model it is assumed that the dielectric medium is made of well conducting grains which are separated by poorly conducting or resistive grain boundaries. Therefore, under application of external electric field, charge carriers easily move from the grains but will be accumulated at

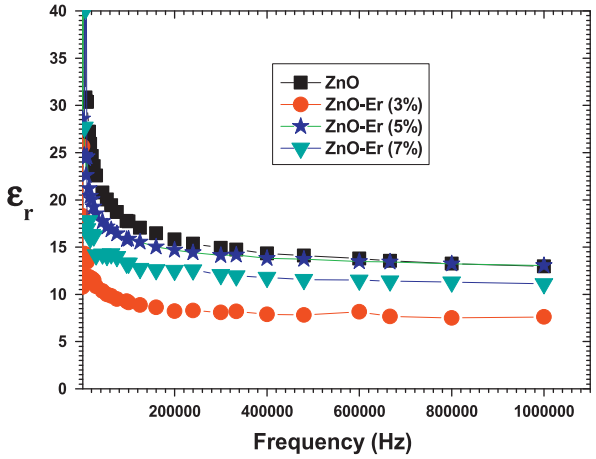

Fig. 5. The dielectric behavior of pure and Er doped ZnO nanostructures in term of frequency.

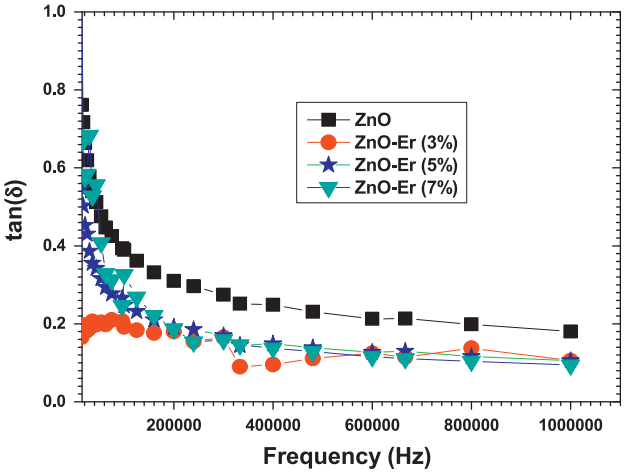

Fig. 6. Variation of loss tangent for pure and Er doped ZnO nanostructures.

the grain boundaries. This process causes large polarization and high dielectric constant produced by the sample. The small conductivity of grain boundary contributes to the high value of dielectric constant at low frequency. The higher value of dielectric constant can also be explained on the basis of interfacial/space charge polarization due to inhomogeneous dielectric structure. The polarization decreases with the increase in frequency and then reaches at a constant value due to the fact that beyond a certain frequency of external field the hopping between different metal ions (Zn^{2+}, Er^{3+}) cannot follow the alternating field. The large value of dielectric constant at lower frequency is due to the predominance of the effects like grain boundary defects, presence of oxygen vacancies, etc. [26], while the decrease in dielectric constant with frequency is natural because of the fact that any species contributing to polarizability is found to show lagging behind the applied field at higher and higher frequencies.

Fig. 6 shows the variation of corresponding dielectric loss (tan δ) values of synthesized pure and ZnO nanostructures as a function of frequency. Loss tangent i.e. tan δ represents the energy dissipation in the dielectric system. It can be seen that, tan δ values decrease with the increase of frequency for all the samples which might be due to the space charge polarization. On the other hand, maximum loss has been obtained for pure ZnO sample which decreases after Er doping and gradually decreases in the higher frequency regime. Therefore, it can be concluded that the Er doped ZnO can be applied for high frequency device applications.

The variation in AC conductivity of all the samples with frequency is shown in Fig. 7. The behavior reveals an increase of the AC conductivity of all the samples with increase of frequency. In general, total conductivity of the sample is described by following equation as [27]:

$$\sigma_{tot} = \sigma_0(T) + \sigma(\omega, T) \quad (1)$$

where, first term corresponds to DC conductivity due to band conduction which is frequency independent and the second term corresponds to pure AC conductivity due to migration of electric charge carriers between the Zn ions. It has been vastly

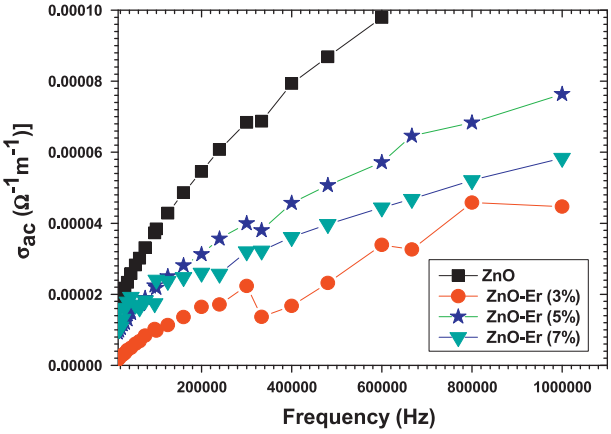

Fig. 7. Variation of AC conductivity for pure and Er doped ZnO nanostructures.

reported in the literature that the AC conductivity gradually increases with the increase in frequency of applied AC field because the increase in frequency enhances the migration of electron. It is also clear from Fig. 7 that the maximum conductivity is obtained for pure ZnO which decreases with Er doping in ZnO. This decrease in AC conductivity can be explained by the fact that Er ions produce defects such as oxygen vacancies and zinc interstitials in the ZnO host system. These defects tend to segregate at the grain boundaries. Therefore, doping increases the defect ions which facilitate the formation of grain boundary defect barrier leading to blockage to the flow of charge carriers. This in turn decreases the conductivity of the system on doping.

4. Conclusion

In summary, Er doped ZnO nanoplates have been successfully synthesized by wet precipitation method. SEM images of the prepared samples clearly reveal the formation of nanoplates like structures with change of morphology from nanorods to nanoplates on Er doping in ZnO. The presence of

two additional phonon modes in Raman spectra at 160 and 620 cm^{-1} for Er doped ZnO samples could be attributed to the local vibration modes due to Er substitution in the ZnO host. Normal dielectric constants and dielectric loss behavior were measured for the prepared nanostructures. AC conductivity of ZnO nanostructures is found to decrease with Er doping. This reduction in conductivity could be due to the presence of zinc interstitials and oxygen vacancies in ZnO matrix on Er doping. Therefore, incorporation of Er ions in ZnO lattice facilitates the formation of grain boundary defect leading to blockage to the flow of charge carriers. This in turn decreases the conductivity of the system on doping.

Acknowledgments

The authors Reza Zamiri and Ajay Kaushal would like to express their personal thanks to FCT (Fundação para a Ciência e a Tecnologia) for post-doctoral research grant with reference numbers (SFRH/BPD/76185/2011) and (SFRH/BPD/77598/2011).

References

[1] R. Zamiri, A. Zakaria, H.A. Ahangar, M. Darroudi, A.K. Zak, G.P. Drummen, Aqueous starch as a stabilizer in zinc oxide nanoparticle synthesis via laser ablation, Journal of Alloys and Compounds 516 (2012) 41–48.
[2] R. Birringer, Nanocrystalline materials, Materials Science and Engineering: A 117 (1989) 33–43.
[3] C. Suryanarayana, Structure and properties of nanocrystalline materials, Bulletin of Materials Science 17 (4) (1994) 307–346.
[4] H. Gleiter, Progress in Materials Science 33 (1989) 223.
[5] J.R. MacDonald, Impedence Spectroscopy—Emphasizing Solid Materials and Systems, Wiley-Interscience, John Wiley and Sons, New York (1987) 1–346.
[6] M. Singhai, V. Chhabra, P. Kang, D. Shah, Synthesis of ZnO nanoparticles for varistor application using Zn-substituted aerosol OT microemulsion, Materials Research Bulletin 32 (2) (1997) 239–247.
[7] S. Hingorani, V. Pillai, P. Kumar, M. Multani, D. Shah, Microemulsion mediated synthesis of zinc-oxide nanoparticles for varistor studies, Materials Research Bulletin 28 (12) (1993) 1303–1310.
[8] R. Viswanath, S. Ramasamy, R. Ramamoorthy, P. Jayavel, T. Nagarajan, Preparation and characterization of nanocrystalline ZnO based materials for varistor applications, Nanostructured Materials 6 (5) (1995) 993–996.
[9] L.F. Dong, Z. Cui, Z. Zhang, Gas sensing properties of nano-ZnO prepared by arc plasma method, Nanostructured Materials 8 (7) (1997) 815–823.
[10] C.W. Nan, S. Holten, R. Birringer, H. Gao, H. Kliem, H. Gleiter, Anomalous space-charge limited currents in nanocrystalline ZnO, Physica Status Solidi (a) 164 (1) (1997) R1–R2.
[11] A.W. Snow, H. Wohltjen, Size-induced metal to semiconductor transition in a stabilized gold cluster ensemble, Chemistry of Materials 10 (4) (1998) 947–949.
[12] J. Lee, J. Hwang, J. Mashek, T. Mason, A. Miller, R. Siegel, Impedance spectroscopy of grain boundaries in nanophase ZnO, Journal of Materials Research 10 (9) (1995) 2295–2300.
[13] D. Zhao, X. Pan, Investigation of optical and electrical properties of ZnO ultrafine particle films prepared by direct current gas discharge activated reactive method, Journal of Vacuum Science and Technology B: Microelectronics and Nanometer Structures 12 (5) (1994) 2880–2883.
[14] H.-M. Zhou, D.-Q. Yi, Z.-M. Yu, L.-R. Xiao, J. Li, Preparation of aluminum doped zinc oxide films and the study of their microstructure, electrical and optical properties, Thin Solid Films 515 (17) (2007) 6909–6914.
[15] S.A. Ansari, A. Nisar, B. Fatma, W. Khan, A. Naqvi, Investigation on structural, optical and dielectric properties of Co doped ZnO nanoparticles synthesized by gel-combustion route, Materials Science and Engineering: B 177 (5) (2012) 428–435.
[16] B. Cao, W. Cai, From ZnO nanorods to nanoplates: chemical bath deposition growth and surface-related emissions, Journal of Physical Chemistry C 112 (3) (2008) 680–685.
[17] D. Chu, S. Li, Growth and electrical properties of doped ZnO by electrochemical deposition, New Journal of Glass and Ceramics 2 (2012) 13–16.
[18] J. Zhang, L. Sun, J. Yin, H. Su, C. Liao, C. Yan, Control of ZnO morphology via a simple solution route, Chemistry of Materials 14 (10) (2002) 4172–4177.
[19] B. Cao, W. Cai, H. Zeng, G. Duan, Morphology evolution and photoluminescence properties of ZnO films electrochemically deposited on conductive glass substrates, Journal of Applied Physics 99 (7) (2006) 073516.
[20] L. Duan, G. Rao, Y. Wang, J. Yu, T. Wang, Magnetization and Raman scattering studies of (Co, Mn) codoped ZnO nanoparticles, Journal of Applied Physics 104 (1) (2008) 013909.
[21] Y. Huang, M. Liu, Z. Li, Y. Zeng, S. Liu, Raman spectroscopy study of ZnO-based ceramic films fabricated by novel sol–gel process, Materials Science and Engineering: B 97 (2) (2003) 111–116.
[22] K. Chen, F.-Y. Hung, S.-J. Chang, Structural characteristic, Raman analysis and optical properties of indium-doped ZnO nanoparticles prepared by sol–gel method, Journal of Nanoscience and Nanotechnology 9 (5) (2009) 3325–3329.
[23] L. Yang, X. Wu, G. Huang, T. Qiu, Y. Yang, In situ synthesis of Mn-doped ZnO multileg nanostructures and Mn-related Raman vibration, Journal of Applied Physics 97 (1) (2005) 014308.
[24] C. Bundesmann, N. Ashkenov, M. Schubert, D. Spemann, T. Butz, E. Kaidashev, M. Lorenz, M. Grundmann, Raman scattering in ZnO thin films doped with Fe, Sb, Al, Ga, and Li, Applied Physics Letters 83 (10) (2003) 1974–1976.
[25] K.W. Wagner, Zur theorie der unvollkommenen dielektrika, Annalen der Physik 345 (5) (1913) 817–855.
[26] I. Gul, A. Abbasi, F. Amin, M. Anis-ur-Rehman, A. Maqsood, Structural, magnetic and electrical properties of $Co_{1-x}Zn_xFe_2O_4$ synthesized by co-precipitation method, Journal of Magnetism and Magnetic Materials 311 (2) (2007) 494–499.
[27] A. Abo El Ata, M. El Nimr, S. Attia, D. El Kony, A. Al-Hammadi, Studies of AC electrical conductivity and initial magnetic permeability of rare-earth-substituted Li–Co ferrites, Journal of Magnetism and Magnetic Materials 297 (1) (2006) 33–43.